A MULTISCALE FEM TO MODEL CO$_2$ SEQUESTRATION IN SALINE AQUIFERS

Gabriela B. Savioli[a]**, Juan E. Santos**[a,b]**, Lucas A. Macias**[a] **and Patricia Gauzellino**[c]

[a]*Universidad de Buenos Aires, Facultad de Ingeniería, Instituto del Gas y del Petróleo, Av. Las Heras 2214 Piso 3 C1127AAR Buenos Aires, Argentina, gsavioli@fi.uba.ar*

[b]*Universidad Nacional de La Plata and, Department of Mathematics, Purdue University, 150 N. University Street, West Lafayette, Indiana, 47907-2067, USA, jsantos48@gmail.com*

[c]*Facultad de Ciencias Astronómicas y Geofísicas,Universidad Nacional de La Plata*

Abstract. A major cause of the attenuation levels observed in seismic data from sedimentary regions is the mesoscopic loss mechanism, caused by heterogeneities in the rock and fluid properties greater than the pore size but much smaller than the wavelengths of the fast compressional and shear waves. The main objective of this paper is to apply a numerical upscaling method to determine the plane wave complex modulus of a viscoelastic solid long-wave equivalent to a fluid saturated poroelastic (Biot's medium) with mesoscopic-scale heterogeneities in the form of brine-CO2 patches. This is achieved by applying time-harmonic compressibility tests at a selected set of frequencies to a representative sample of bulk material. These tests are modeled as boundary value problems stated in the space-frequency domain. This numerical upscaling approach was applied using data from the CO2 sequestration Sleipner-field case. A numerical flow simulator to represent the CO2 injection and storage was combined with a wave propagation model in order to obtain synthetic seismograms. The flow and petrophysical parameters were determined to obtain synthetic seismograms resembling actual field data. The simulations yield CO2 accumulations below the mudstone layers and synthetic seismograms which successfully match the typical pushdown effect, observed in actual field data.

1 INTRODUCTION

Recent results have demonstrated the importance of the mesoscopic effects in the context of exploration geophysics, being the dominant P-wave attenuation mechanism in reservoir rocks at seismic frequencies (Pride et al., 2004). Basically, when a compressional wave squeezes an heterogeneous fluid-saturated porous material, the different regions of the medium, due to their distinct elastic properties, may undergo different strains and fluid pressures. This in turn produces fluid flow and Biot's slow waves generating energy loss and velocity dispersion.

White and coauthors (White et al., 1975; White, 1975) were the first to model the wave-induced fluid flow produced by mesoscopic-scale heterogeneities, showing that this mechanism can produce important attenuation and velocity dispersion effects at seismic frequencies in partially saturated rocks. They obtained approximated solutions of the response of plane porous layers alternately saturated with gas and water (White et al., 1975) and of spherical gas pockets in a water-saturated porous rock (White, 1975). Since then, many authors have made very important contributions to a better understanding of this subject (Pride and Berryman, 2003; Johnson, 2001; Norris, 1993; Gurevich and Lopatnikov, 1995). The major drawback of these analytical theories is that they can only be used in the case of heterogeneities having idealized geometries. Mesoscopic effects have also been studied by performing numerical simulation of wave propagation (Helle et al., 2003). This is a more versatile approach since one may model heterogeneities of any kind and shape, but is computationally expensive or even not feasible. The methodology used in this work obtains the effective plane wave complex modulus of heterogeneous rock samples by defining an equivalent viscoelastic solid with the same attenuation and velocity dispersion as the original fluid-saturated porous rock. This is achieved by applying time-harmonic compressibility stresses to a representative sample of bulk material, which are mathematically modeled as local boundary value problems stated in the space-frequency domain. Biot's equation in the diffusive range is used to model the response of the heterogeneous material to the applied stresses, and the approximate solution is obtained using a finite-element procedure.

We test this methodology using data from the CO_2 sequestration site in the Utsira formation at the Sleipner field. The only field data available is a collection of seismic sections (time-lapse seismics) used to monitor the CO_2 storage procedure. An estimate of the CO_2 injection rate and the location of the injection point are known. Using these data we build a geological model, including intramudstone layers with openings, whose coordinates are defined by using the field seismic data. We also model fractal variations of the petrophysical properties. The numerical simulation of the CO_2-brine flow is based on the Black-Oil formulation. The flow simulator parameters and the petrophysical properties are updated to obtain CO_2 saturation maps, including CO_2 plumes. Then, we compute synthetic seismograms on the basis of the resulting saturation and pore-pressure maps. Wave attenuation and velocity dispersion are included using the above described methodology, obtaining an equivalent viscoelastic medium at the macroscale. The wave equation is solved in the space-frequency domain for a collection of frequencies in the range of interest with a finite-element iterative domain decomposition algorithm. The space-time solution is recovered by a discrete inverse Fourier transform.

The numerical examples illustrate the success of the combined application of the flow and wave propagation simulators to model the CO_2 storage procedure in the Utsira formation at the Sleipner field, in particular representing the pushdown effect observed in field data.

2 METHODOLOGY

2.1 CO$_2$ - brine flow model in porous media

The well-known Black-Oil formulation applied to two-phase, two component fluid flow (Aziz and Settari, 1985) is used to simulate the simultaneous flow of brine (subindex o) and CO$_2$ (subindex g), considering that CO$_2$ may dissolve in the brine but the brine is not allowed to vaporize into the CO$_2$ phase. This formulation uses the PVT data (CO$_2$ solubility in brine; CO$_2$ and brine formation volume factors) as a simplified thermodynamic model. The solution of the Black-Oil model is obtained employing the public domain software BOAST (Fanchi, 1997) which solves the differential equations using the IMPES (IMplicit Pressure Explicit Saturation) finite difference technique.

2.2 Modeling of the mesoscopic attenuation effects at the mesoscale

Let $\mathbf{u}_s$ and $\tilde{\mathbf{u}}_f$ denote the averaged displacement vectors of the solid and fluid phases, respectively. Let $\mathbf{u}_f = \phi(\tilde{\mathbf{u}}_f - \mathbf{u}_s)$ be the relative fluid displacement, where ϕ denotes the porosity and set $\mathbf{u} = (\mathbf{u}_s, \mathbf{u}_f)$. Let $\varepsilon(\mathbf{u}_s)$, $\tau(\mathbf{u})$ and $p_f(\mathbf{u})$ denote the strain tensor of the solid, the stress tensor of the bulk material and the fluid pressure, respectively. The stress-strain relations are (Biot, 1962):

$$\tau_{st}(\mathbf{u}) = 2G\,\varepsilon_{st}(\mathbf{u}_s) + \delta_{st}(\lambda_U \nabla \cdot \mathbf{u}_s + \alpha\, M \nabla \cdot \mathbf{u}_f), \tag{1}$$

$$p_f(\mathbf{u}) = -\alpha\, M \nabla \cdot \mathbf{u}_s - M \nabla \cdot \mathbf{u}_f. \tag{2}$$

G is the shear modulus of the dry matrix. The other coefficients in (1)-(2) can be obtained in terms of K_s, K_m and K_f, the bulk moduli of the solid grains, dry matrix and saturant fluid, respectively (Carcione, 2007).

Biot's equations in the diffusive range and in the absence of external forces are (Biot, 1962):

$$\nabla \cdot \tau(\mathbf{u}) = 0, \tag{3}$$

$$\mathrm{i}\omega\mathbf{u}_f + \frac{\mu}{\kappa}\nabla p_f(\mathbf{u}) = 0, \tag{4}$$

where $\mathrm{i} = \sqrt{-1}$, ω is the angular frequency, μ is the fluid viscosity and κ is the frame permeability.

A very convenient approach to study mesoscopic effects is to apply time-harmonic compressional stresses to a representative sample of a fluid-saturated porous rock, which enables us to obtain its *equivalent* complex plane-wave modulus. This is performed by defining an equivalent viscoelastic medium with the same attenuation and velocity dispersion as the original porous rock. The theoretical basis for this procedure were given in the works of (White, 1975; Dutta and Odé, 1979; Johnson, 2001).

To perform this test, we solve equations (3)-(4) under convenient boundary conditions. Denote by ν the unit outer normal on Γ, the boundary of the domain, and let χ be a unit tangent on Γ oriented counterclockwise so that $\{\nu, \chi\}$ is an orthonormal system on Γ.

To determine the complex plane wave modulus of our fluid-saturated porous medium, let us consider the solution of (3)-(4) with the following boundary conditions

$$\tau(\mathbf{u})\nu \cdot \nu = -\Delta P, \quad (x_1, x_3) \in \Gamma^T, \tag{5}$$

$$\tau(\mathbf{u})\nu \cdot \chi = 0, \quad (x_1, x_3) \in \Gamma, \tag{6}$$

$$\mathbf{u}^s \cdot \nu = 0, \quad (x_1, x_3) \in \Gamma^L \cup \Gamma^R \cup \Gamma^B, \tag{7}$$

$$\mathbf{u}^f \cdot \nu = 0, \quad (x_1, x_3) \in \Gamma. \tag{8}$$

where Γ^L, Γ^R, Γ^B and Γ^T are the left, right, bottom and top boundaries of the domain, respectively. For this set of boundary conditions the solid is not allowed to move normally to the lateral and bottom boundaries, the fluid is not allowed to flow out of the sample, a uniform compression is applied on the boundary Γ^T and no tangential external forces are applied on the boundary Γ.

Denoting by V the original volume of the sample, its (complex) oscillatory volume change $\Delta V(\omega)$ allows us to define the *equivalent* undrained complex plane-wave modulus $M_c(\omega)$, by using the relation

$$\frac{\Delta V(\omega)}{V} = -\frac{\Delta P}{M_c(\omega)}, \tag{9}$$

valid for a viscoelastic homogeneous medium in the quasistatic case.

Then, for each frequency ω, the complex volume change produced by the compressibility test can be approximated by

$$\Delta V(\omega) \approx L u_3^{s,T}(\omega),$$

which enables us to compute the *effective* complex plane-wave modulus $M_c(\omega)$ from (9).

The corresponding complex compressional velocity is $V_{pc}(\omega) = \sqrt{\frac{M_c(\omega)}{\overline{\rho}_b}}$, where $\overline{\rho}_b$ is the average bulk density of the sample.

Next, the following relations allow us to estimate the effective compressional phase velocity $V_p(\omega)$ and quality factor $Q_p(\omega)$ in the form:

$$V_p(\omega) = \left[\text{Re}\left(\frac{1}{V_{pc}} \right) \right]^{-1} \qquad \frac{1}{Q_p(\omega)} = \frac{\text{Im}(V_{pc}^2)}{\text{Re}(V_{pc}^2)} \tag{10}$$

In order to estimate this equivalent complex plane wave modulus $M_c(\omega)$, we use a finite-element procedure to approximate the solution of the equations of motion (3)-4 with the boundary conditions 5-8.

We use bilinear functions to approximate the solid displacement vector, while a closed subspace of the vector part of the Raviart-Thomas-Nedelec space of zero order (Raviart and Thomas, 1975; Nedelec, 1980) for the fluid displacement is employed. It can be demonstrated that the error associated with this numerical procedure measured in the energy norm is of order $h^{1/2}$.

2.3   Seismic Modeling: A viscoelastic model for wave propagation

The equation of motion in a 2D isotropic viscoelastic domain Ω with boundary $\partial\Omega$ is (Santos et al., 2011) :

$$\omega^2 \rho u + \nabla \cdot \sigma(u) = f(x, \omega), \quad \Omega, \tag{11}$$

with boundary condition:

$$-\sigma(u)\nu = i\omega \mathcal{D} u, \quad \partial\Omega. \tag{12}$$

Here $f(x, \omega)$ is the external source and $\mathcal{D}$ is a positive definite matrix which definition is given in (Ha et al., 2002).

The numerical solution is computed at a selected number of frequencies in the range of interest using an iterative finite element domain decomposition procedure. The time domain solution is obtained using a discrete inverse Fourier transform (Ha et al., 2002) . To approximate each component of the solid displacement vector we employ a nonconforming finite element space which generates less numerical dispersion than the standard bilinear elements.

3   NUMERICAL RESULTS

We consider a model of the Utsira formation having 1.2 km in the x-direction, 10 km in the y-direction and 0.4 km in the z-direction (top at 0.77 km and bottom at 1.17 km b.s.l.). Within the formation, there are several mudstone layers which act as barriers to the vertical motion of the CO_2. The initial porosity ϕ is assumed to have a fractal spatial distribution based on the so-called von Karman self-similar correlation functions (Santos et al., 2005), and horizontal and vertical permeabilities are determined from porosity using the relations described in (Santos et al., 2014). CO_2 is injected during five years in the Utsira formation at a constant flow rate of one million tons per year. The injection point is located at the bottom of the formation: $x = 0.6$ km, $z = 1.082$ km. Figure 1 shows 2D vertical slices (corresponding to $n_y = 3$) of the CO_2 saturation fields after five years of CO_2 injection. CO_2 accumulations below the mudstone layers can be observed. As injection proceeds, part of the injected fluid migrates upwards due to the openings in the mudstone layers that generate chimneys.
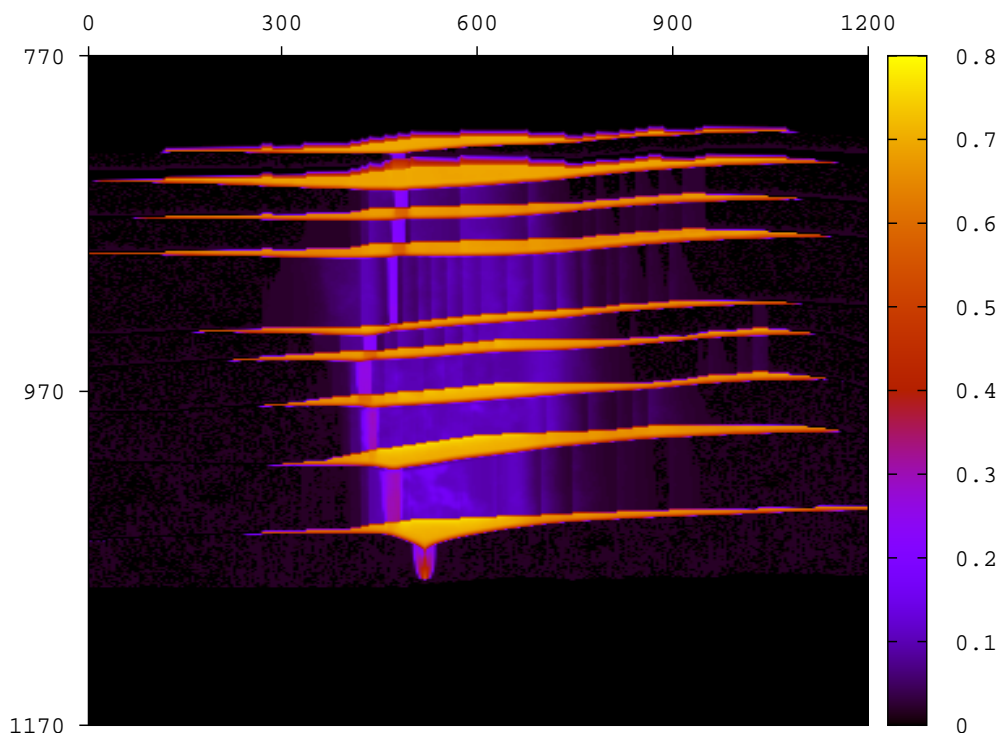
Figure 1: CO_2 saturation distribution after five years of CO2 injection

We analyze the capability of seismic monitoring to identify zones of CO_2 accumulation and migration. With this purpose, we use 2D slices of CO_2 saturation and fluid pressure obtained from the flow simulator to construct a 2D model of the Utsira formation. The seismic source is a spatially localized plane wave of main frequency 60 Hz.

In order to compute the equivalent complex plane-wave modulus for each saturation, we consider a porous sample with a spatially variable gas - water distribution in the form of irregular *patches* fully saturated with gas and zones fully saturated with water. No mixing forces are taken into account and the two fluids are assumed to occupy different mesoscopic regions of the model. The generation of these kind of distributions involves the use of a stochastic fractal field

(Santos et al., 2005). To illustrate this, in Figures 2 and 3 we show patches for 0.05 and 0.3 of CO_2 saturation.
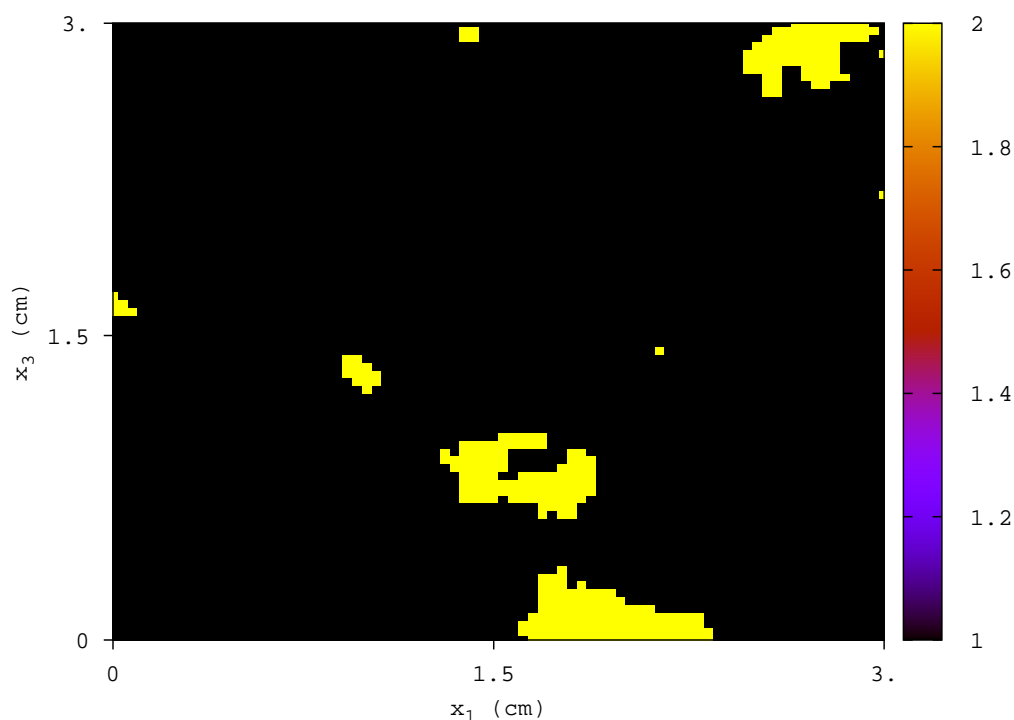
Figure 2: Patchy water-gas distributions for overall CO_2 saturation $S_g = 0.05$. The yellow zones correspond to 100 % gas saturation and the black zones to 100 % water saturation

Figures 4 and 5 display fluid pressure maps at frequencies of 1 Hz and 50 Hz, respectively. Both maps correspond to patchy water-gas distributions for overall CO_2 saturation $S_g = 0.30$ (Figure 3). We can observe that pressure is lower in zones of 100 % CO_2 saturation. Besides, comparing both figures, as time proceeds higher pressure values are obtained.

Figure 6 displays the seismogram after five years of CO_2 injection associated with the CO_2 saturations shown in Figure 1. A standard f-k filter is applied to the seismic sections. The reflections seen in those seismograms show the CO_2 accumulations below the mudstone layers as the injection proceeds. In particular, the pushdown effect observed in the real seismograms of Figure 7 (Chadwick et al., 2005) due to CO_2 accumulations is clearly observed.

4   CONCLUSIONS

We describe a methodology to deal with the mesoscopic loss mechanism. It is based on the finite element solution of the classical Biot's equations to simulate oscillatory compressibility tests, obtaining the complex effective plane wave modulus for different saturations. Unlike the theoretical White's theory valid only for periodic alternating layers, our method allows to simulate any kind of heterogeneities within the domain. Our results indicate that in the frequency range analyzed the complex effective plane wave modulus is very sensitive to the overall gas saturation. The fluid-flow simulator yields CO_2 accumulations below the mudstone layers and the corresponding synthetic seismograms resemble the real seismic data, where the pushdown effect is clearly observed.
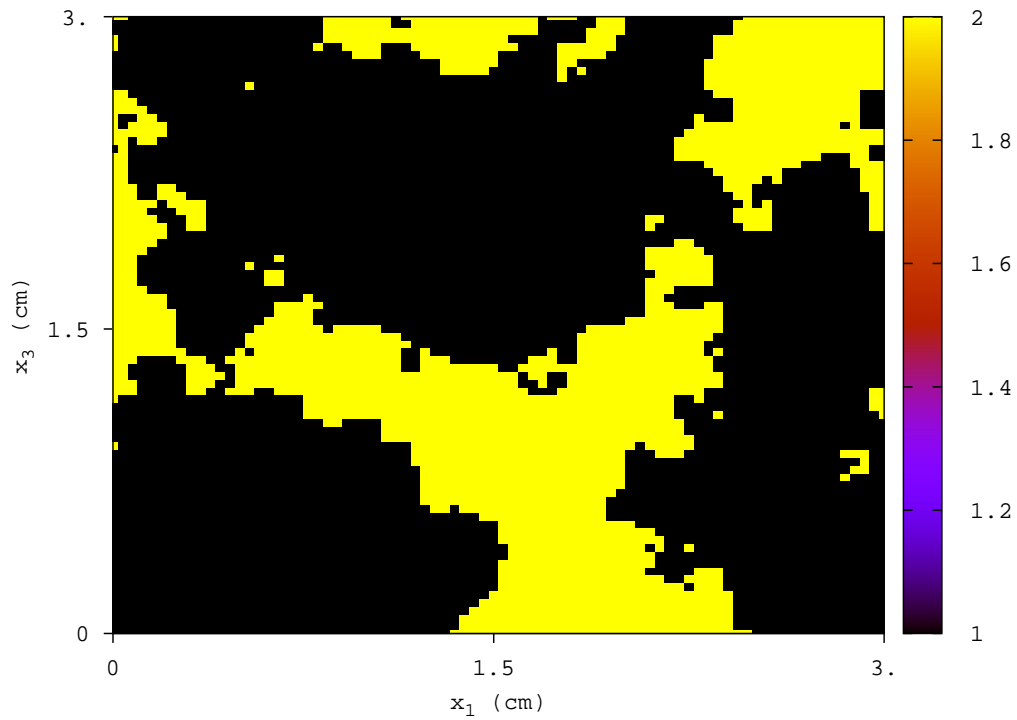
Figure 3: Patchy water-gas distributions for overall CO_2 saturation $S_g = 0.30$. The yellow zones correspond to 100 % gas saturation and the black zones to 100 % water saturation
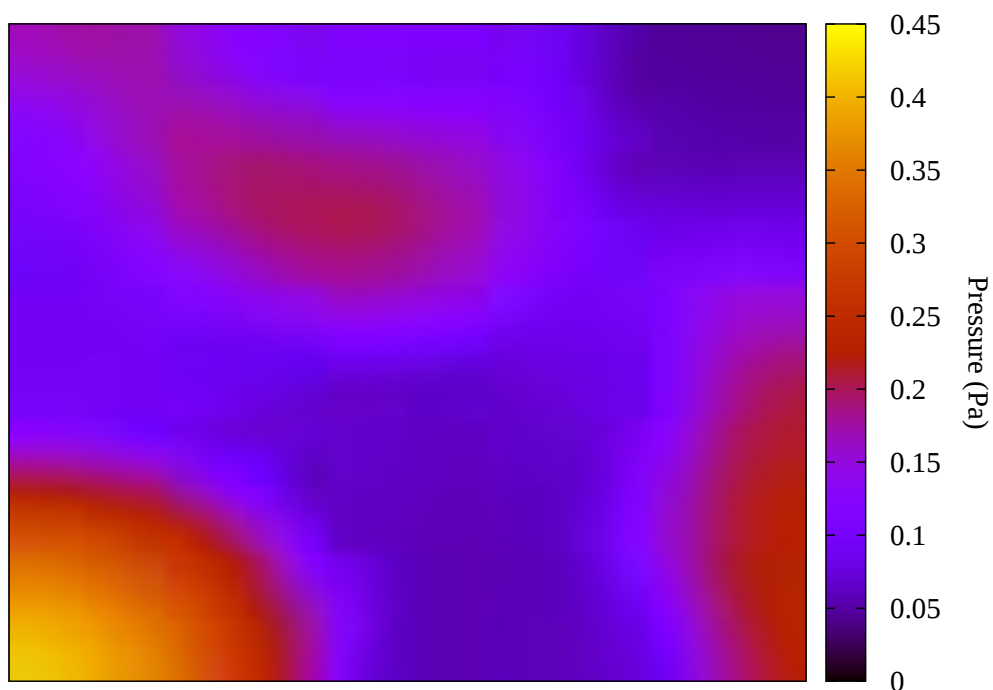
Figure 4: Fluid pressure map at frequency of 1 Hz, corresponding to patchy water-gas distributions for overall CO_2 saturation $S_g = 0.3$
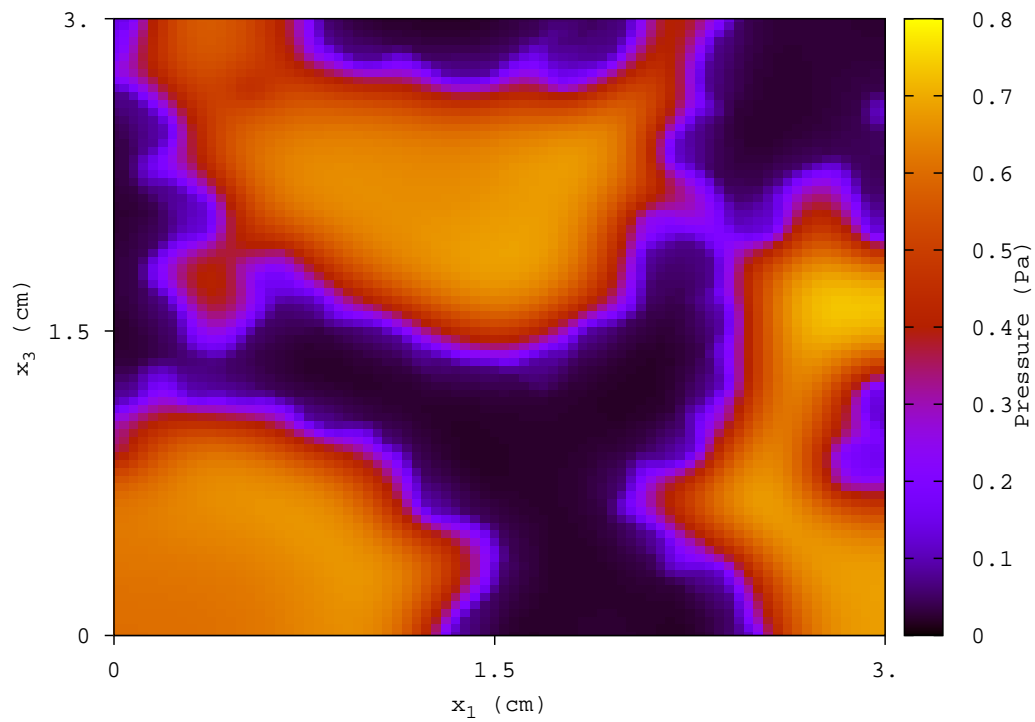
Figure 5: Fluid pressure map at frequency of 50 Hz, corresponding to patchy water-gas distributions for overall CO_2 saturation $S_g = 0.3$

5 ACKNOWLEDGMENTS
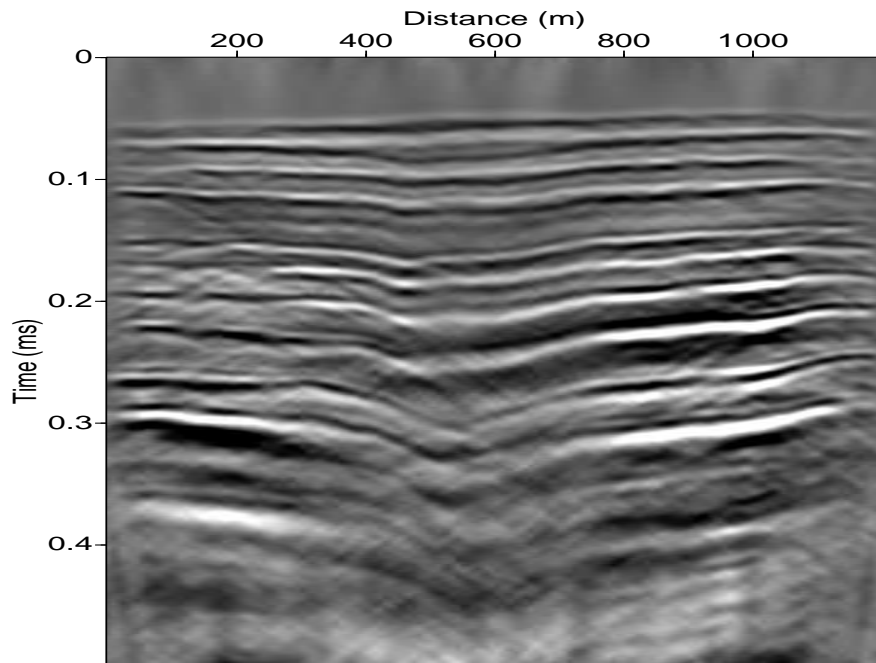
Figure 6: Synthetic seismogram after five years of CO2 injection
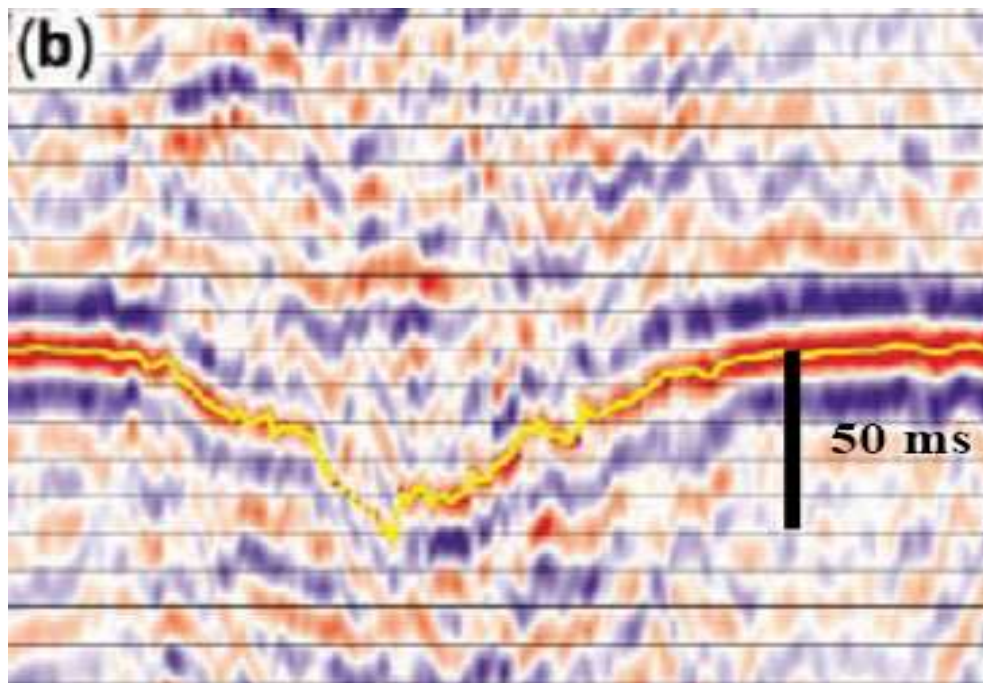
Figure 7: Real cross-correlogram after 5 years (Chadwick et al., 2005)

REFERENCES

Aziz K. and Settari A. *Petroleum Reservoir Simulation*. Elsevier Applied Science Publishers, Great Britain, 1985.

Biot M. Mechanics of deformation and acoustic propagation in porous media. *Journal of Applied Physics*, 33:1482–1498, 1962.

Carcione J.M. *Wave fields in real media: Wave Propagation in Anisotropic, Anelastic, Porous and Electromagnetic Media, Handbook of Geophysical Exploration, vol. 38*. Elsevier (2nd edition, revised and extended), 2007.

Chadwick A., Arts R., and Eiken O. 4d seismic quantification of a growing CO_2 plume at sleipner, north sea. *Dore A G and Vincent B (Eds) Petroleum Geology: North West Europe and Global Perspectives - Proc. 6th Petroleum Geology Conference*, pages 1385–1399, 2005.

Dutta N.C. and Odé H. Attenuation and dispersion of compressional waves in fluid-filled porous rocks with partial gas saturation (White model) – Part I: Biot theory. *Geophysics*, 44:1777–1788, 1979.

Fanchi J. *Principles of Applied Reservoir Simulation*. Gulf Professional Publishing Company, Houston, Texas, 1997.

Gurevich B. and Lopatnikov S. Velocity and attenuation of elastic waves in finely layered porous rocks. *Geophysical Journal International*, 121:933âĂŞ947, 1995.

Ha T., Santos J., and Sheen D. Nonconforming finite element methods for the simulation of waves in viscoelastic solids. *Comput. Meth. Appl. Mech. Engrg.*, 191:5647–5670, 2002.

Helle H., Pham N., and Carcione J. Velocity and attenuation in partially saturated rocks: poroelastic numerical experiments. *Geophysical Prospecting*, 51:551–566, 2003.

Johnson D. Theory of frequency dependent acoustics in patchy-saturated porous media. *Journal of the Acoustical Society of America*, 110:682âĂŞ694, 2001.

Nedelec J.C. Mixed finite elements in $\mathbf{R}^3$. *Numer. Math.*, 35:315–341, 1980.

Norris A. Low-frequency dispersion and attenuation in partially saturated rocks. *Journal of the Acoustical Society of America*, 94:359âĂŞ370, 1993.

Pride S. and Berryman J. Linear dynamics of double-porosity and dualpermeability materials. i. governing equations and acoustic attenuation. *Physical Review E*, 68:036603, 2003.

Pride S., Berryman J., and Harris J. Seismic attenuation due to waveinduced flow. *Journal of Geophysical Research*, 109:B01201, 2004.

Raviart P.A. and Thomas J.M. Mixed finite element method for 2nd order elliptic problems. *Mathematical Aspects of the Finite Element Methods, Lecture Notes of Mathematics, vol. 606, Springer*, 1975.

Santos J., Ravazzoli C., Gauzellino P., and Carcione J. Numerical simulation of ultrasonic waves in reservoir rocks with patchy saturation and fractal petrophysical properties. *Computational Geosciences*, 9:1–27, 2005.

Santos J., Savioli G., Macias L., Carcione J., and Gei D. Influence of capillary pressure on co2 storage and monitoring. *Proc. 84th Annual International Meeting SEG (Denver)*, 2014.

Santos J.E., Carcione J.M., and Picotti S. Analysis of mesoscopic loss effects in anisotropic poroelastic media using harmonic finite element simulations. *Proc. 81th Annual International Meeting SEG (San Antonio)*, pages 2211–2215, 2011.

White J.E. Computed seismic speeds and attenuation in rocks with partial gas saturation. *Geophysics*, 40:224–232, 1975.

White J.E., Mikhaylova N.G., and Lyakhovitskiy F.M. Low-frequency seismic waves in fluid-saturated layered rocks. *Izvestija Academy of Siences USSR, Physics of Solid Earth*, 10:654–659, 1975.